Revision 2

Insights into the structure of mixed CO_2/CH_4 in gas hydrates

S. Michelle Everett[1,*], Claudia J. Rawn[1,2,†], Bryan C. Chakoumakos[3], David J. Keffer[1], Ashfia Huq[3], and Tommy J. Phelps[4]

[1]Department of Materials Science and Engineering, University of Tennessee, Knoxville, TN 37996-2100, U.S.A.

[2]Materials Science and Technology Division, Oak Ridge National Laboratory, Oak Ridge, TN 37831-6475, U.S.A.

[3]Quantum Condensed Matter Division, Oak Ridge National Laboratory, Oak Ridge, TN 37831-6475, U.S.A.

[4]Biosciences Division, Oak Ridge National Laboratory, Oak Ridge, TN 37831-6475, U.S.A.

[*]S.M. Everett is now a member of the Scientific Activities Division, European Spallation Source, Lund, Sweden, michelle.everett@esss.se

[†]Corresponding author: crawn@utk.edu

ABSTRACT

The exchange of carbon dioxide for methane in natural gas hydrates is an attractive approach to harvesting CH_4 for energy production while simultaneously sequestering CO_2. In addition to the energy and environmental implications, the solid solution of clathrate hydrate $(CH_4)_{1-x}(CO_2)_x \cdot 5.75H_2O$ provides a model system to study how the distinct bonding and shapes of CH_4 and CO_2

influence the structure and properties of the compound. High-resolution neutron diffraction was used to examine mixed CO_2/CH_4 gas hydrates. CO_2-rich hydrates had smaller lattice parameters, which were attributed to the higher affinity of the CO_2 molecule interacting with H_2O molecules that form the surrounding cages, and resulted in a reduction in the unit cell volume. Experimental nuclear scattering densities illustrate how the cage occupants and energy landscape change with composition. These results provide important insights on the impact and mechanisms for the structure of mixed CH_4/CO_2 gas hydrate.

KEYWORDS

Neutron diffraction, methane hydrate, carbon dioxide/methane exchange, Fourier density maps

INTRODUCTION

The search for energy sources to ease environmental and political issues of conventional sources has encouraged scientists to look to the sun, the plants, and the ocean for answers. Found at moderate pressure, low temperature conditions such as the ocean floor and subsurface permafrost regions, natural gas hydrates constitute a valuable potential source of methane (Koh and Sloan 2007, Makogon 2007). The amount of carbon stored in natural gas hydrates is estimated to be twice that of all other carbon sources combined (Suess et al. 1999). Over the past 15 years the idea of harvesting methane from natural hydrate deposits while simultaneously sequestering industrially produced CO_2 has been tantalizing (Brewer et al. 1999, Lee et al. 2003, Qi et al. 2011, Ripmeester and Ratcliffe 1998, Ohgaki et al. 1996, Ota et al. 2005). As envisioned, CO_2 is pumped deep into the sediment layers where natural hydrates are found. The CO_2 replaces CH_4 in the hydrate structure, and CH_4 is released. This conceptually simple

process involves great engineering challenges, and a detailed understanding of the crystallographic response to the mixture of CO_2 and CH_4 molecules in gas hydrate formation is key to understanding the implications of a large-scale adoption of this strategy.

Gas hydrates are structures comprised of differently shaped cages formed from water molecules, which are stabilized by encapsulated gas molecules. Methane hydrate most commonly adopts cubic structure type I (sI) (Schicks and Ripmeester 2004), as does CO_2. Two small cages and six large cages of hydrogen-bonded water molecules make up the sI clathrate hydrate unit cell. The ideal ratio is 8 gas molecules to 46 water molecules, but may not necessarily be the case due to the fact that they are nonstoichiometric compounds. Figure 1 shows how a large and small cage fit together. CO_2 hydrate is more thermodynamically stable at temperatures below 283 K (Ohgaki et al. 1996, Anderson et al. 2003, Kang et al. 1998) than CH_4 hydrate, and the stability of CO_2 hydrate requires less pressure at a given temperature than CH_4 (~2 MPa at 277 K vs. ~4 MPa for CH_4 hydrate (Adisamito et al. 1991, Adisamito and Sloan 1992)). Molecular dynamics simulation found the Gibbs free energy for CO_2 gas exchange in CH_4 hydrate is negative (Yezdimer et al. 2002), indicating it is thermodynamically favorable to replace CH_4 with CO_2 in gas hydrate (Geng et al. 2009). Yuan et al. (2012) proposed that CO_2 exchange takes place by a reconstructive transformation, whereby the CH_4 hydrate first dissociates, and then the water reforms hydrate choosing from the dissolved mixture of CO_2/CH_4 gas. Shicks et al. (2011) reported the process was a decomposing and reforming process, which is driven by the chemical potential gradient between gas phase and hydrate phase. The placement and cage occupancy of the gas molecules during this process dictates the change in structure, which is relevant for seafloor stability prediction.

Studies were performed where CH_4 hydrate was exposed to CO_2 and the recovery results reported, which indicated it was a slow process (Lee et al. 2003, Schicks et al. 2011, Hirohama 1996, Park et al. 2006). It is conceivable to envision that a solid solution range develops during this replacement process affecting the structure of the formation. In this study, we examined the structural changes of sI gas hydrates as compared to each end-member via high-resolution neutron diffraction over a CH_4/CO_2 hydrate solid solution series. Samples were synthesized from liquid water and CO_2 and CH_4 gas. Using this synthesis route, the preference of the two cage types for one gas or the other could be established in the hydrate formation process. Samples of each end-member as well as 3:1, 1:1, and 1:3 CH_4/CO_2 target ratios were synthesized and studied to establish a comparison across the composition range.

EXPERIMENTAL

Sample synthesis

10 mL of liquid D_2O (Sigma Aldrich 99.9%) was mixed with 1 mg of Snomax,® an ice nucleating protein made from *Pseudomonas syringae 31a*, previously reported to decrease the formation pressure (McCallum et al. 2007). This solution was then placed in a 450 mL Parr vessel with steel bars used for milling media. The vessel was sealed and evacuated. Each sample was pressurized with gas to 4.13 MPa (600 psi). There were 5 samples with initial gas mixtures of 100% CH_4, 75% CH_4/25% CO_2, 50% CH_4/50% CO_2, 25% CH_4/75% CO_2, and 100% CO_2. In the mixed samples CO_2 was introduced first to 1.03, 2.07, and 3.10 MPa (150, 300, and 450 psi), immediately followed by CH_4 to achieve a total pressure of 4.13 MPa. The pressure vessel was stored in a cold room at 275 K on a tumbler and was tumbled constantly for ~5 days at 30 RPM. For the 100% CO_2 sample at 275 K and 4.13 MPa the CO_2 would be liquid. The

pressure drop associated with hydrate formation was monitored and hydrate formation was assumed to be complete when the pressure stopped dropping. Samples were then stored at 253 K until they were depressurized, quenched in liquid nitrogen, harvested, and stored in liquid nitrogen. While the samples were synthesized using D_2O, the CH_4 was not deuterated (i.e. not CD_4) and was isotopically natural. This choice creates a natural contrast in the measurements; the atomic scattering density for H has an opposite sign from the atomic scattering density for O, creating a strong contrast between CH_4 from CO_2 as guest occupants.

Neutron data collection

Samples were loaded into vanadium cans (OD = 10 mm). Neutron powder diffraction data were collected at the Spallation Neutron Source at Oak Ridge National Laboratory on the POWGEN time-of-flight diffractometer. Data were collected using wavelength bands centered at 1.333 Å and 2.665 Å providing a range from 0.42 to 6.18 Å in d-spacing. In attempt to decrease the molecular motion and atomic vibrations and to collect data at ambient pressure without any complications associated with decomposition, data were collected at 10 K. To avoid solid N_2 at this temperature, the V cans were evacuated and backfilled with chilled He, 3 to 4 times. It was successful for 4 of the 5 samples. In the one sample solid N_2 was present at < 7 wt% of the total sample.

POWGEN was chosen for its high-resolution capabilities along with the availability of high Q data. High Q data are imperative for resolving low d-spacing peaks, which are needed to model nearly freely rotating gas molecules with no primary chemical bonding to the crystalline lattice, and to determine details including occupant types, abundance of occupants, and atomic displacement parameters (ADPs). Figure 2 shows the observed data, calculated neutron powder

diffraction pattern and the difference pattern for the 50% CH_4 sample. A low d-spacing section is shown illustrating the high-resolution. Inelastic neutron scattering has previously shown that the methane molecules in methane hydrate are almost freely rotating (Gutt et al. 1999, Kamiyama et al. 2006, Tse et al. 1997) and neutron powder diffraction has shown that CO_2 molecules in CO_2 hydrate have a restricted but unresolved libration and large displacements (Ikeda et al. 1999). This study shows real-space, static depictions of distributions of the nuclear scattering densities in both the large and small cages by way of Fourier transforms of the diffraction data, and the extended Q-range data from POWGEN ensures high fidelity. Experimental specifics are given in Table 1.

Rietveld refinements

GSAS (Larson and Von Dreele 1994) along with EXPGUI (Toby 2001) were used for Rietveld refinements of the data. In the refinements, a rigid body treatment of the gas molecules was employed. A rigid body fixes the atoms of a molecule to be bound together at certain bond lengths and angles allowing the molecule to be treated as a discrete unit (Lake and Toby 2011). This is beneficial for reducing the number of refineable parameters, resulting in refinements less influenced by statistical uncertainty. The movement of the molecule was then handled by TLS tenors (translation, libration, and screw) instead of individual vectors for each atom of the molecule. The high symmetry of sI hydrate's space group, *Pm-3n* (223), further reduced the number of TLS elements. Once the rigid bodies were defined, the occupancies of the rigid bodies were refined. At first the occupancies were constrained to hold the cages fully occupied in a 3:1 ratio LC:SC. Subsequently the site occupancy factor was refined; the restraint was

relaxed to allow for determination of vacancies and the residuals decreased. Specifics on the refinements can be found in Table 2.

RESULTS AND DISCUSSION

The results from Fourier difference analysis were exported for use in VESTA (Momma and Izumi 2011) to provide graphical visualizations of the gas molecules. For the visualizations, the host lattice was accounted for in the refinement model while the gas molecules were removed from the model, so that the Fourier difference map revealed the nuclear scattering density distributions within the cages (Fig. 3a,b). These maps represent a time average of the nuclear density of the molecules inside the clathrate structure over the collection time, which is a real space approach (Takeya et al. 2011) to hydrate analysis through gas visualization. The C and O atoms both have positive bound coherent scattering lengths, while the H scattering length is negative (6.6460(12), 5.803(4), -3.7390(11) fm (Sears 1992), respectively). The density maps, with positive scattering density in yellow and negative in blue, clearly indicate the occupants in the large cages and the small cages, and verify that for the end-member samples only CO_2 or CH_4 exist in the cages. The nuclear density maps for the end-member samples provide reference points of comparison for the three mixed-gas samples. A blending of the mixed gases and their decreasing CH_4 content is evident in the morphing of the nuclear density maps from one end-member to the other. Gas molecules are superimposed on the nuclear density maps to give a spatial sense of the map relationship to the molecules themselves. The large cages appeared to confine CO_2 molecules to {010} planes of motion due to cage shape, size and surface potential restrictions, but the more symmetrical small cage allowed the CO_2 molecule to move equally in all directions. Methane appeared to be free to oscillate isotropically in either size cage, which is

160 expected given its smaller molecular van der Waals radius and tetrahedral shape (Sloan and Koh
161 2007).

162 The density maps show little evidence of CH_4 in the large cage of the nominal 25% CH_4
163 sample. By comparing the maps side by side it can be seen that the large cages of all mixed
164 samples show reduced CH_4, while the small cages show less CO_2. This is explained by the tight
165 fit of CO_2 in the small cage (Lee et al. 2003), making CH_4 more favorable to the small cage and
166 CO_2 more favorable to the large cage. Table 3 contains the refinement results of the site
167 occupancies for the guest molecules, supporting the visually identified gas mixtures and cage
168 occupants. Overall greater percentages of CH_4 are in the small cages and greater percentages of
169 CO_2 are in the large ones. These results also confirm that not all cages are completely filled
170 throughout the structure resulting in hydration numbers, determined by $n = 46/(6\theta_L + 2\theta_S)$ where
171 θ is the cage occupancy (Qin and Kuhs 2013), of 7.19(4), 8.21(4), 6.93(4), 6.12(3), 5.75(3) for
172 100% CH_4, 75% CH_4, 50% CH_4, 25% CH_4, and 100% CO_2, respectively. The 100% occupancy
173 for the 100% CO_2 sample could be due to the CO_2 synthesis occurring with the CO_2 in the liquid
174 state, when cooled down to 275 K and 4.13 MPa, as compared to the gaseous state for the mixed
175 samples. Vacancies in both sized cages, and evidence of a higher percentage of CO_2 in the
176 smaller cage than expected, illustrate structural changes that could occur in the hydrate reservoir
177 during gas exchange. Additionally, these results have important implications for computational
178 studies of gas hydrates since the amount and location of the gas molecules are important starting
179 parameters for theoretical models.

180 From thermodynamics, one can model the mixed CH_4-CO_2 hydrate as an azeotropic
181 system (Bakker, 1998). This model illustrates that under specific conditions the gas hydrate is
182 enriched in CO_2 compared to the gas mixture, but there are also conditions where the reversed

183 behavior occurs. However, this approach cannot predict the distribution of gas molecules
184 between the small and large cages. The CSMHYD software (Sloan 1998) can and was used to
185 predict site occupancies using the quench temperature of 253 K and the results are given in Table
186 4. Comparing the predicted site occupancies (Table 4) with the experimentally refined site
187 occupancies (Table 3) show that CSMHYD (Sloan 1998) always predicts a higher site
188 occupancy for the CH_4 content in the larger cages and a higher CH_4 content overall as compared
189 to the experimental results. For the 100%, 75%, and 50% CH_4 samples the experimentally
190 determined amount of total cages occupied is significantly lower while the experimental
191 determined amount of total cages occupied for the 25% and 0% CH_4 samples are within 1σ of
192 the values predicted by CSMHYD (Sloan 1998). Factors that could have contributed to the
193 difference between the experimentally refined and predicted site occupancies include changes
194 that could have occurred while the samples were being stored at atmospheric pressure and 77 K
195 and contributions from incoherent scattering for the samples with higher hydrogen content. Other
196 reports have shown higher cage occupancies in methane hydrate as well, ~95 – 97% (Lee et al.
197 2003, Qin and Kuhs 2013, Ripmeester and Ratcliffe 1988). Sum et al. (1997) reported a higher
198 occupancy of CH_4 in both large and small cages as temperatures increased, possibly explaining
199 the lower occupancy seen here at 10 K. The predicted stability pressures, also shown in Table 4,
200 are well below the 4.13 MPa used to synthesize the samples.
201 Figure 4a shows the variations of lattice parameters with the experimentally refined CH_4
202 composition. The lattice parameter decreases with a Vegard's Law type behavior as the CH_4
203 content decreases, resulting in a 0.25% reduction in unit cell volume from the CH_4 hydrate end-
204 member to the CO_2 hydrate end-member, contrary to the expectation that the lattice parameters
205 would increase as the amount of the larger CO_2 molecule increased, when considering the van

der Waals radii of these two gases (Sloan and Koh 2007). One plausible explanation for this anomalous behavior could be attributed to greater atomic displacement parameters, ADPs, for the smaller, lighter molecule. Due to a smaller molecular mass and tetrahedral shape, the CH_4 molecule should be able to move more freely (Kuhs 1992) and to push on the structure causing it to expand. Again an anomalous behavior was observed, and larger ADPs were refined for the CO_2 hydrate end-member (Fig. 4b). The refined ADPs for the CO_2 molecules occluded in the large cages are significantly larger than the ADPs refined for the CH_4 molecules contained in either the large cage or small cage. At the same time, the refined ADPs for the CO_2 molecules in the small cages are only slightly larger than those refined for the CH_4 molecules contained in either the large cages or small cages.

ADPs are highly correlated with both site occupancy and absorption correction. Disorder can be an additional complicating consideration in these systems especially considering the random 50% occupation of the D atoms in the host lattice and the almost freely rotating gas molecules of mixed gases. By comparing the refined ADPs of the large cage and the percentage of cages that are full, the large cage ADPs decrease from the CO_2 hydrate end-member to 75% CO_2/25% CH_4 nominal composition, as does the overall cage occupancy, from 100(6)% - 70(3)%. However, both the refined ADPs and cage occupancies start to increase for the CH_4 hydrate end-member, indicating the strong relation between ADPs and molecular movement in the structure.

The claim that the ADPs are influencing the lattice parameters is based on entropic arguments in which the energy landscape within the cage is relatively constant, allowing the occluded species to explore the entirety of the cage volume. This assumption is valid for CH_4, which is a non-polar molecule, resulting in weak energetic interactions with the framework water

molecules. Consequently, the shape of the adsorption site for CH_4 (Fig. 3c) is approximately spherical, mimicking the shape of the cage. The same assumption is not valid for CO_2, which has a permanent quadrupole, resulting in a non-negligible energetic interaction with the framework. Moreover, previous work has shown that a significant portion of the large displacement of the CO_2 molecule is due to its positional disorder in the large cage (Circone et al. 2003).

When energetics are important, the ADPs are not only guided by molecular weight or cage size, but are dominated by adsorption site size, defined by the energy landscape within the cage. This behavior can be seen in the nuclear density maps (Fig. 3c). The CO_2 nuclear density volumes in the large cages are anisotropic and do not mimic the shape of the cage. As the isosurface level is increased to the point that only the energy maxima sites are shown, one observes that for CO_2 the ADP is averaging localization in 4 distinct sites. The anisotropy of the CO_2 molecule is evident in the multiple views, where it exhibits a disc type probability distribution. On the other hand, the CH_4 is much more spherical and shows no preferred sites, thus explaining the larger ADP of the CO_2. The electrostatic attraction between CO_2 and H_2O may also serve to reduce the lattice constant for the CO_2 hydrate, pulling in the water matrix as it bounces between the 4 maxima. The energy landscape in the small cage is not as influential, because both CO_2 and CH_4 are isotropic in that site. Another interesting anomaly is that the volumes of large cages and small cages do not increase uniformly with increasing lattice size. Large cage volume increases with increasing CH_4 content, while small cage volume decreases (Fig. 4c, d). Small cages have the largest volume in the CO_2 hydrate end-member sample, again pointing to the tight fit of CO_2, and large cages have the largest volume when they contain the smaller CH_4 molecule. Klapproth et al. (2003) reported an overall larger cage volume ratio

252 V_{SC}/V_{LC} for CO_2 over CH_4, explained by the larger small cage of CO_2, where we find them to be
253 approximately the same, 0.69 for CH_4 and 0.70 for CO_2, due to the large cage compensation.
254 Large cages dominate the structure by a 3:1 ratio, so their increase in volume dictates the overall
255 increase of the lattice parameters as the CH_4 content increases.

256 The occupants of the cages play a role in the density of the structure (Fig. 4e). The hydrate
257 becomes denser than seawater at ~30% CH_4 when calculated using the formula weight
258 determined from the refined site occupancies and the refined unit cell volumes. Using a
259 Vegard's law extrapolation of the lattice parameters to estimate volume of a completely filled
260 H_2O structure, the transition occurs at a much higher percentage of CH_4, ~70%. This outcome
261 indicates that the vacancies of the cages and the preference for CO_2 in the structure are
262 significant structural factors when estimating the resulting physical behavior during exchange.
263 The experimental densities indicate that the solid solution is denser than seawater at a much
264 smaller CO_2 content than would be expected for the ideal solution with full cage occupancies.
265 These structural changes must be anticipated and considered when dealing with changing
266 properties of large amounts of hydrate in the seafloor.
267

268 **IMPLICATIONS**

269 In this synthesis, where mixed hydrates were formed with liquid water and CO_2/CH_4 in
270 gas phase, the D_2O host network can select gas molecules from the headspace during hydrate
271 formation, suggesting a strong preference of gas occupants based on the gas mixture present at
272 the time of formation. These occupants set the tone for the overall structure. Significant
273 deviations from an ideal solid solution are found. The behavior of CO_2 and CH_4 in the large
274 cage are quite different due to both energetic and entropic effects. Energetically, the permanent

quadrupole of CO_2 results in a stronger guest-host interaction. Entropically, CO_2 exhibits a distinctly non-spherical adsorption site within the large cage. These factors impact not only the relative occupancies of CH_4 and CO_2 but the hydrate lattice parameters and unit cell volume as well. This study and future studies similar to it will facilitate better exchange models for predicting outcomes when recovering CH_4 from natural gas hydrates and exchanging the CH_4 molecules with CO_2 molecules for CO_2 sequestering. This method of synthesis and neutron diffraction characterization provide a powerful combination to vary composition and temperature of mixed gas hydrates for solid solution determinations and structural, volumetric physical property changes, thus paving the way for successful exchange that allows utilization of natural gas hydrates for CO_2 sequestration and clean energy production.

ACKNOWLEDGMENTS

SME was supported by National Science Foundation Grant No. DGE0801470, "Sustainable Technology through Advanced Interdisciplinary Research" (STAIR), awarded to the University of Tennessee Knoxville. Oak Ridge National Laboratory is managed by UT-Battelle LLC, for the US Department of Energy, which provided support of the Spallation Neutron Source through the Scientific User Facilities Division, Office of Basic Energy Sciences, and additional support by the Office of Fossil Energy through Field Work Proposal FEAB111 "Hydrate Formation and Dissociation in Simulated and Field Samples."

REFERENCES

Adisasmito, S., Frank, R.J., and Sloan, E.D. (1991) Hydrates of carbon dioxide and methane mixtures. Journal of Chemical & Engineering Data, 36, 68-71.

298 Adisasmito, S. and Sloan, E.D. (1992) Hydrates of hydrocarbon gases containing carbon dioxide.
299 Journal of Chemical & Engineering Data, 37, 343-349.
300 Anderson, R., Llamedo, M., Tohidi, B., and Burgass, R.W. (2003) Experimental measurement of
301 methane and carbon dioxide clathrate hydrate equilibria in mesoporous silica. Journal of
302 Physical Chemistry B, 107, 3507-3515.
303 Bakker, R.J. (1998) Improvements in clathrate modeling II: the H2O-CO2-CH4-N2-C2N6 fluid
304 system. Geological Society, London, Special Publications, 137, 75-104.
305 Brewer, P.G., Friederich, C., Peltzer, E.T., and Orr, F.M. (1999) Direct experiments on the ocean
306 floor disposal of fossil fuel CO_2. Science, 284, 943-945.
307 Circone, S., Stern, L.A., Kirby, S.H., Durham, W.B., Chakoumakos, B.C., Rawn, C.J.,
308 Rondinone, A.J., and Ishii, Y. (2003) CO_2 hydrate: synthesis, composition, structure,
309 dissociation behavior, and a comparison to structure I CH4 hydrate. Journal of Physical
310 Chemistry B, 107, 5529-5539.
311 Geng, C.Y., Wen, H., and Zhou, H. (2009) Molecular simulation of the potential of methane
312 reoccupation during the replacement of methane hydrate by CO_2. Journal of Physical
313 Chemistry A, 113, 5463-5469.
314 Gutt, C., Asmussen, B., Press, W., Merkl, C., Casalta, H., Greinert, J., Bohrmann, G., Tse, J.S.,
315 and Huller, A. (1999) Quantum rotations in natural methane clathrates from the Pacific
316 seafloor. Europhysics Letters, 48, 269-275.
317 Hirohama, S., Shimoyama, Y., Wakabayashi, A., Tatsuta, S., and Nishida, N. (1996) Conversion
318 of CH_4 hydrate to CO_2 hydrate in liquid CO_2. Journal of Chemical Engineering of Japan,
319 29, 1014-1020.

Ikeda, T., Yamamuro, O., Matsuo, T., Mori, K., Torii, S. Kamiyama, T., Izumi, F., Ikeda, S., and Mae, S. (1999) Neutron diffraction study of carbon dioxide clathrate hydrate. Journal of Physics and Chemistry of Solids, 60, 1527-1529.

Kamiyama, T., Seki, N., Iwasa, H., Uchida, T., Ebinuma, T., Narita, H., Igawa, N., Ishii, Y., Bennington, S.M., and Kiyanagi, Y. (2006) Methane molecular motion in clathrate hydrate host framework. Physica B Condensed Matter, 385, 202-204.

Kang, S.P., Chun, M.K., and Lee, H. (1998) Phase equilibria of methane and carbon dioxide hydrates in the aqueous $MgCl_2$ solutions. Fluid Phase Equilibria, 147, 229-238.

Klapproth, A., Goreshnik, E., Staykova, D., Klein, H., and Kuhs, W.F. (2003) Structural studies of gas hydrates. Canadian Journal of Physics, 81, 503-518.

Koh, C.A. and Sloan, E.D. (2007) Natural gas hydrates: Recent advances and challenges in energy and environmental applications. AIChE Journal, 53, 1636-1643.

Kuhs, W.F. (1992) Generalized atomic displacements in crystallographic structure analysis. Acta Crystallographica Section A: Foundations of Crystallography, 48, 80-98.

Lake, C.H. and Toby, B.H. (2011) Rigid body refinements in GSAS/EXPGUI. Powder Diffraction, 26, S13-S21.

Larson, A.C. and Von Dreele, R.B. (1994) General Structure Analysis System (GSAS). Los Alamos National Laboratory Report, LAUR 86-748.

Lee, H., Seo Y., Seo, Y.T., Moudrakovski, I.L., and Ripmeester, J.A. (2003) Recovering methane from solid methane hydrate with carbon dioxide. Angewandte Chemie-International Edition, 42, 5048-5051.

Makogon, Y., Holditch, S.A., and Makogon, T.Y. (2007) Natural gas hydrates – A potential energy source for the 21st century. Journal of Petroleum Science and Engineering, 56, 14-31.

McCallum, S.D., Riestenberg, D.E., Zatsepina, O.Y., and Phelps, T.J. (2007) Effect of pressure vessel size on the formation of gas hydrates. Journal of Petroleum Science and Engineering, 56, 54-64.

Momma, K. and Izumi, F (2011) VESTA 3 for three-dimensional visualization of crystal, volumetric and morphology data. Journal of Applied Crystallography, 44, 1272-1276.

Ohgaki, K., Takano, K., Sangawa, H., Matsubara T., and Nakano, S. (1996) Methane exploitation by carbon dioxide from gas hydrates – Phase equilibria for CO_2 – CH_4 mixed hydrate system. Journal of Chemical Engineering of Japan, 29, 478-483.

Ota, M., Morohashi, K., Abe, Y., Watanabe, M., Smith, R.L., and Inomata, H. (2005) Replacement of CH_4 in the hydrate by use of liquid CO_2. Energy Conversion and Management, 46, 1680-1691.

Park, Y., Kim, D.Y., Lee, J.W., Huh, D.G., Park, K.P., Lee, J., and Lee, H. (2006) Sequestering carbon dioxide into complex structures of naturally occurring gas hydrates. Proceedings of the National Academy of Sciences of the United States of America, 103, 12690-12694.

Qi, Y.X., Ota, M., and Zhang, H. (2011) Molecular dynamics simulation of replacement of CH_4 in hydrate with CO_2. Energy Conversion and Management, 52, 2682-2687.

Qin, J.F. and Kuhs, W.F. (2013) Quantitative analysis of gas hydrates using Raman spectroscopy. AIChE Journal, 59, 2155-2167.

Ripmeester, J.A. and Radcliffe, C.I. (1988) Low-temperature cross-polarization/magic angle spinning carbon-13 NMR of solid methane hydrates: Structure, cage occupancy, and hydration number. The Journal of Physical Chemistry, 92, 337-339.

Ripmeester, J.A. and Ratcliffe, C.I. (1998) The diverse nature of dodecahedral cages in clathrate hydrates as revealed by Xe-129 and C-13 NMR spectroscopy: CO_2 as a small-cage guest. Energy & Fuels, 12, 197-200.

Schicks, J.M. and Ripmeester, J.A. (2004) The coexistence of two different methane hydrate phases under moderate pressure and temperature conditions: Kinetic versus thermodynamic products. Angwwandte Chemie-International Edition, 43, 3310-3313.

Schicks, J.M., Luzi, M., and Beeskow-Strauch, B. (2011) The conversion process of hydrocarbon hydrates into CO_2 hydrates and vice-versa: Thermodynamic considerations. Journal of Physical Chemistry A, 115, 13324-13331.

Sears, V.F. (1992) Neutron scattering lengths and cross sections. Neutron News, 3, 26-37.

Sloan, E.D. and Koh, C.A. (2007) Clathrate Hydrates of Natural Gases, 3rd ed. Taylor & Francis CRC Press, Boca Raton, FL.

Sloan, E.D. (1998) Clathrate Hydrates of Natural Gases. Marcel Dekker, New York.

Suess, E., Bohrmann, G., Greinert, J., and Lausch, E. (1999) Flammable Ice. Scientific American, 281, 76-83.

Sum, K.A., Burruss, R.C., and Sloan, E.D. (1997) Measurement of clathrate hydrates via Raman spectroscopy. Journal of Physical Chemistry B, 101, 7371-7377.

Takeya, S., Yoneyama, A., Ueda, K., Hyodo, K., Takeda, T., Mimachi, H., Takahashi, M., Iwasaki, T., Sano, K., Yamawaki, H., and Gotoh, Y. (2011) Nondestructive imaging of

anomalously preserved methane clathrate hydrate by phase contrast x-ray imaging. Journal of Physical Chemistry C, 115, 16193-16199.

Toby, B.H. (2001) EXPGUI, a graphical user interface for GSAS. Journal of Applied Crystallography, 34, 210-213.

Tse, J.S., Ratcliffe, C.I., Powell, B.M., Sears, V.F., and Handa, Y.P. (1997) Rotational and translational motions of trapped methane: Incoherent inelastic neutron scattering of methane hydrate. Journal of Physical Chemistry A, 101, 4491-4495.

Yezdimer, E.M., Cummings, P.P., and Chialvo, A.A. (2002) Determination of the Gibbs free energy of gas replacement in sI clathrate hydrates by molecular simulation. Journal of Physical Chemistry A, 106, 7982-7987.

Yuan, Q., Sun, C.Y., Yang, X., Ma, P.C., Ma, Z.W., Liu, B., Ma, Q.L., Yang, L.Y., and Chen G.J. (2012) Recovery of methane from hydrate reservoir with gaseous carbon dioxide using a three-dimensional middle-size reactor. Energy, 40, 47-58.

399 Table 1. Experimental information for neutron powder data collected on five hydrate samples
400 with nominal gas amounts of 100% CH_4, 75% CH_4/25% CO_2, 50% CH_4/50% CO_2, 25%
401 CH_4/75%CO_2, 100% CO_2.

Refined Chemical Formula	0.79(CH_4) 7.19H_2O	0.36(CH_4) 0.34(CO_2) 8.21H_2O	0.2(CH_4) 0.63(CO_2) 6.93H_2O	0.08(CH_4) 0.85(CO_2) 6.12H_2O	(CO_2) 5.75H_2O
Crystal system	cubic	cubic	cubic	cubic	cubic
Space group	$Pm\bar{3}n$	$Pm\bar{3}n$	$Pm\bar{3}n$	$Pm\bar{3}n$	$Pm\bar{3}n$
a (Å)	11.83210(8)	11.82699(4)	11.82487(6)	11.82427(7)	11.82216(9)
Volume (Å^3)	1656.48	1654.34	1653.44	1653.19	1652.31
ρ_{calc} (g/cm^3)	0.93	1.00	1.08	1.14	1.19
Temperature (K)	10	10	10	10	10
Phases	97% hyd, 3% ice I	90% hyd, 10% ice I	92% hyd, 8% ice I	90% hyd, 7% ice I, 3% N_2	99% hyd, 1% ice I

402

403

Table 2. Crystallographic goodness of fit information for neutron powder data collected on five hydrate samples with nominal gas amounts of 100% CH_4, 75% CH_4/25% CO_2, 50% CH_4/50% CO_2, 25% CH_4/75% CO_2, 100% CO_2.

Refined Chemical Formula	$0.79(CH_4)\ 7.19H_2O$		$0.36(CH_4)\ 0.34(CO_2)\ 8.21H_2O$		$0.2(CH_4)\ 0.63(CO_2)\ 6.93H_2O$	
Center wavelength	1.333	2.665	1.333	2.665	1.333	2.665
d-spacing range	0.57-3.59	1.23-6.16	0.66-3.59	1.15-6.16	0.66-3.59	1.15-6.16
Rp	0.009	0.011	0.022	0.032	0.025	0.034
Rwp	0.010	0.012	0.022	0.032	0.024	0.035
Rexp	0.002	0.003	0.003	0.004	0.003	0.004
χ^2	5.72	3.81	7.10	7.69	9.38	8.16
Combined Rp	0.010		0.028		0.030	
Combined Rwp	0.011		0.026		0.028	
Variables	36		47		47	
Refined Chemical Formula	$0.08(CH_4)\ 0.85(CO_2)\ 6.12H_2O$		$(CO_2)\ 5.75H_2O$			
Center wavelength	1.333	2.665	1.333	2.665		
d-spacing range	0.57-3.59	1.23-6.16	0.66-3.59	1.15-6.16		
Rp	0.009	0.011	0.022	0.032		
Rwp	0.010	0.012	0.022	0.032		
Rexp	0.002	0.003	0.003	0.004		
χ^2	5.72	3.81	7.10	7.69		
Combined Rp	0.010		0.028			
Combined Rwp	0.011		0.026			
Combined Rwp	36		47			

Table 3. Refined cage occupancies are shown for each molecule and each cage with nominal gas amounts of 100% CH_4, 75% CH_4/25% CO_2, 50% CH_4/50% CO_2, 25% CH_4/75% CO_2, 100% CO_2. The refined cage occupancies are applied to the 2 small cages and 6 large cages to calculate the percent of each gas present. The final column shows the percentage of all cages filled.

Target	Large Cage Occ.		Small Cage Occ.		Content %		% Cages
Composition	CH_4	CO_2	CH_4	CO_2	CH_4	CO_2	Full
100% CH_4	0.73(3)	-	0.93(5)	-	79(4)	-	79(4)
75% CH_4	0.28(2)	0.42(1)	0.59(3)	0.09(2)	36(2)	34(1)	70(3)
50% CH_4	0.08(3)	0.77(1)	0.54(4)	0.21(2)	20(3)	63(1)	83(5)
25% CH_4	0.00(2)	0.98(2)	0.33(4)	0.47(3)	8(3)	85(2)	94(5)
0% CH_4	-	1.00(6)	-	1.00(4)	-	100(6)	100(6)

Table 4. Cage occupancies as predicted using CSMHYD (Sloan 1998) for samples with nominal gas amounts of 100% CH_4, 75% CH_4/25% CO_2, 50% CH_4/50% CO_2, 25% CH_4/75% CO_2, 100% CO_2. The predicted cage occupancies are applied to the 2 small cages and 6 large cages in order to calculate the percent of each gas present. The final column shows the minimum pressure at which the structure would be stable.

Composition	Large Cage Occ.		Small Cage Occ.		Content %		% Cages	Pressure
	CH_4	CO_2	CH_4	CO_2	CH_4	CO_2	Full	(kPa)
100% CH_4	0.98	-	0.90	-	96	-	96	1401
75% CH_4	0.46	0.52	0.67	0.19	51	44	95	975
50% CH_4	0.23	0.76	0.45	0.37	29	66	95	762
25% CH_4	0.09	0.89	0.22	0.56	12	81	93	632
0% CH_4	-	0.98	-	0.75	-	92	92	544

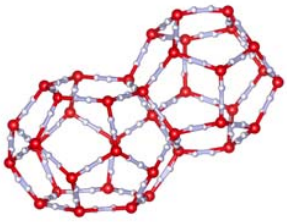

Figure 1. Two polyhedral cages (large cage on left, small cage on right) defined by the hydrogen bonded water network in sI hydrate VESTA (Momma and Izumi 2011). The vertices are the locations of the oxygen atoms (red) and the edges are hydrogen sites (white) randomly half occupied.

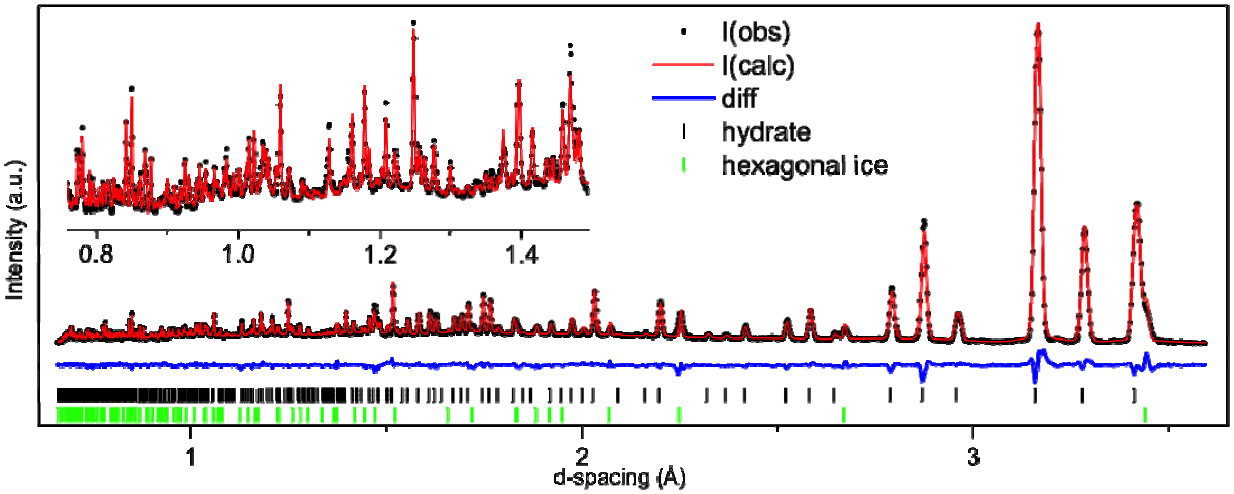

Figure 2. Observed, calculated, and difference neutron powder diffraction patterns for 50% CO_2/50% CH_4 feed gas sample. 0.75 – 1.5 Å has been enlarged to show the resolvability of the low d-spacing range.

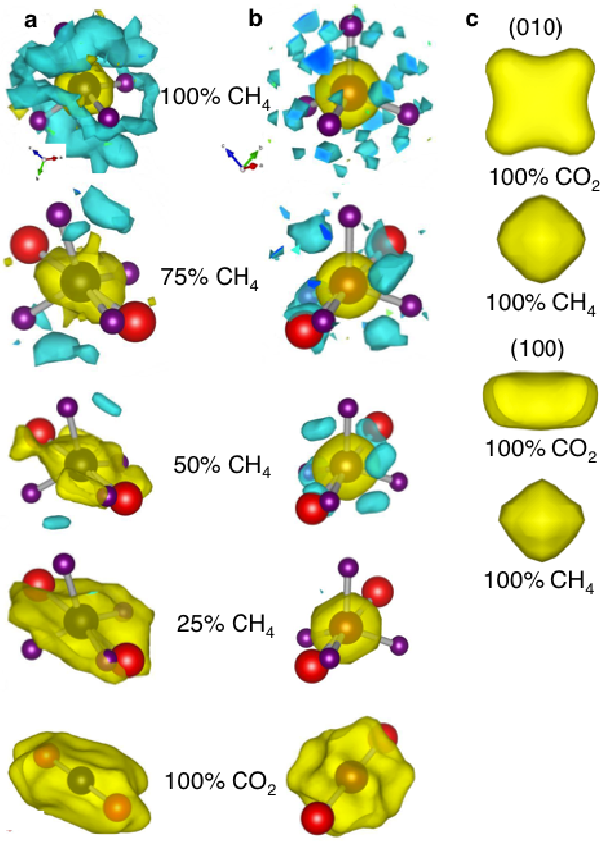

Figure 3. Nuclear densities of large and small cages as determined by Fourier difference analysis of CO_2/CH_4 gas hydrate created in VESTA (Momma and Izumi 2011). Large cages depicted on the left (a) and small cages on the right (b). The isosurface level is 1.5 fm/Å^3 for last four samples (nominal compositions of 75% CH_4, 50% CH_4, 25% CH_4, and 100% CO_2), and 2.2 fm/Å^3 for nominal composition 100% CH_4 (to eliminate extra noise created by high incoherent scattering from hydrogen). Positive nuclear scattering (oxygen and carbon) is shown in yellow, negative (hydrogen) in blue. A single CO_2 and/or CH_4 molecule is superimposed to give a spatial sense of the molecule compared to the observed nuclear density. Energy maxima determined from the nuclear density for the large cage (c) with isosurface level 3 fm/Å^3; CO_2 top, CH_4 bottom, shown along both the {010} and {100} projections in the large cage to demonstrate the extent of the anisotropy of CO_2 distribution on this site.

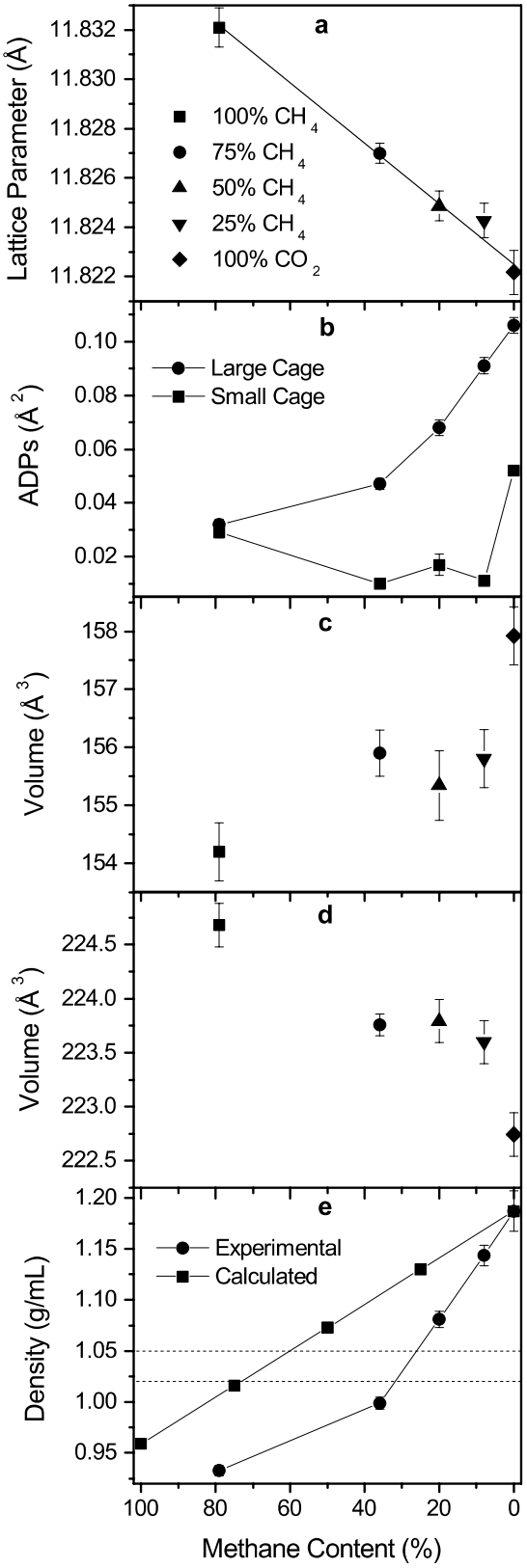

450

Figure 4. Refined lattice parameters (a) and refined atomic displacement parameters (b). Volumes of the small cages (c) and large cages (d) calculated from refined atomic coordinates. The top legend denotes the sample names as they correspond to the nominal feed gas composition. Experimental densities determined from the refined occupancies and calculated densities for the nominal compositions (e) comparing how the density changes based on the guest molecule. Error bars in a, b, c, and d are 3σ and the errors were propagated to obtain the error bars for e.